ASP Conference Series, Vol. 73, 1995
M.R. Haas, J.A. Davidson, and E.F. Erickson (eds.)

SPECTRAL IMAGING OF THE ORION BAR AT 6.2 AND 7.8 MICRONS

Jesse Bregman and David Harker
MS 245-6, NASA Ames Research Center, Moffett Field, CA 94035-1000

David Rank and Pasquale Temi
UCO and UCSC, Santa Cruz, CA 95064

ABSTRACT We have obtained images of the Orion Bar region through narrow-band filters at 6.2 and 7.8 μm to determine whether the emission observed at these wavelengths arises from C-C modes in polycyclic aromatic hydrocarbons (PAHs). Morphologically, the distribution of the emissions are similar, but appear different in detail. Quantitative comparisons of these band intensities with previous data at 8.4 and 11.3 μm indicates that they are indeed consistent with emission from fluorescently excited PAH molecules.

INTRODUCTION

The set of narrow emission bands and broad underlying plateaus which dominate the mid-infrared spectrum of planetary nebulae, HII regions, galactic nuclei, reflection nebulae, and WC stars are generally attributed to material containing only carbon and hydrogen atoms. Several forms of this material have been suggested, but they all are dominated by aromatic carbon structures. The narrow bands are most likely due to emission from polycyclic aromatic hydrocarbons (PAHs), while the broad plateaus arise from larger amorphous carbon particles or PAH clusters. If the narrow features are due to PAHs, then PAHs contain about 1% of the interstellar carbon, making them the most abundant molecules after H_2 and CO. Thus, deciphering the physics of these molecules and their spectra could lead to an understanding of some of the organic chemistry of the interstellar medium.

OBSERVATIONS

The Ames/Lick mid-IR camera was used to image the Orion Bar region at 6.2 and 7.8 μm (PAH features) and 6.8 μm (continuum). The camera uses a 128x128 Si:Ga Amber Engineering array. A filter wheel holding a 4-8 μm CVF and 4 fixed filters determines the wavelength of the image. The 6.2 and

6.8 μm images were obtained through the $\lambda/\delta\lambda$=1.8% CVF while the 7.8 μm image was obtained through a $\lambda/\delta\lambda$=2.5% wide fixed filter. The Bar was chopped 4 arcmin in azimuth at a frequency of 1/3 Hz. Each integration consisted of the difference of 20 on-source and off-source frames. The scale was 1.6 arcsec/pixel. Telescope motion produced FWHM images of point sources of about 4 pixels. Guiding was relative to Θ^2Ori. The telescope was operated in its rotation freeze mode where field rotation is compensated by rotation of the line-of-sight axis. This method held the rotation constant for about 6 integrations. Derotation of the frames for coaddition was done after the flight during image processing.

DISCUSSION

C-C Modes

Previously, Bregman et al. (1994) had shown that the spatial distribution of the emission bands observable from the ground (3.3, 11.3 μm, and a point at 8.4 μm on the long wavelength wing of the 7.7 μm band) could be described by a quantitative model of PAH emission calculated by Schutte et al. (1993). In the PAH model, the 3.3 and 11.3 μm bands are due to C-H modes while the 6.2 and 7.8 μm bands are due to C-C modes. Thus, airborne observations were required to observe the C-C modes and find out if they also fitted the PAH model.

Since the 6.2 and 7.8 μm bands are close in wavelength (and therefore in excitation energy) and are supposed to be due to the same modes in the same molecules, to first order they should have the same spatial distribution. Inspection of the images shows that they are similar, but there are differences in the details of their intensity distribution. We also wanted to confirm that the 8.4 μm image we previously obtained was a good indicator of emission from the C-C modes of PAHs. To do these tests quantitatively, we used the technique we developed in our previous work. In Figures 1a, 1b, and 1c we have plotted the intensity of the bands attributed to C-C modes relative to each other. We use averages of rows of pixels parallel to the front of the Bar and extending from the northern side (next to the HII region) to the southern side (next to the molecular cloud) of the Bar, since in this direction the molecules within the Bar experience a large variation of UV flux and, hence, show a large variation in intensity. On each figure, the solid line is the trend expected if the band intensities are proportional. All the data points should lie along this line if the spatial distribution of the bands are the same. Also plotted are the direction and magnitude of deviations from this line predicted by the PAH model of Schutte et al. (1993). Their standard model has been normalized to the observed intensity of the mid-Bar pixels.

The 7.8 and 6.2 μm data (Fig. 1a) do not correlate 1:1. The points along the front and back of the Bar deviate from the 1:1 trend line in a direction consistent with either a distribution of larger molecules than in the middle of the Bar or with lower UV flux. We observed similar trends in our previous data, with the points along the front of the Bar showing emission characteristic of larger PAHs and the points along the back of the Bar

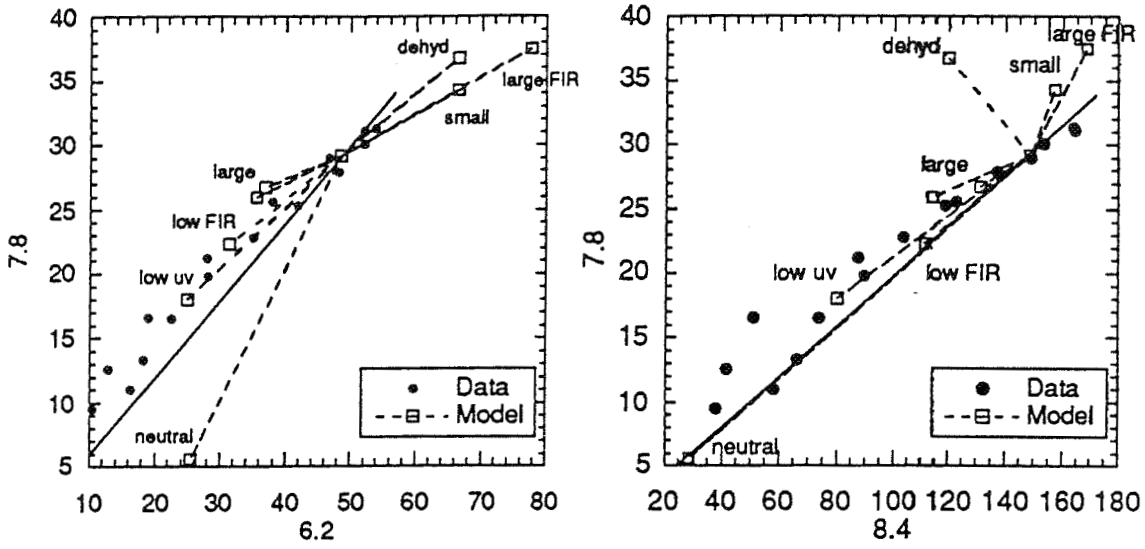

Figure 1 a (left) and Figure 1b (right) show the correlation between the C-C mode band intensities as measured at 6.2, 7.8, and 8.4 microns.

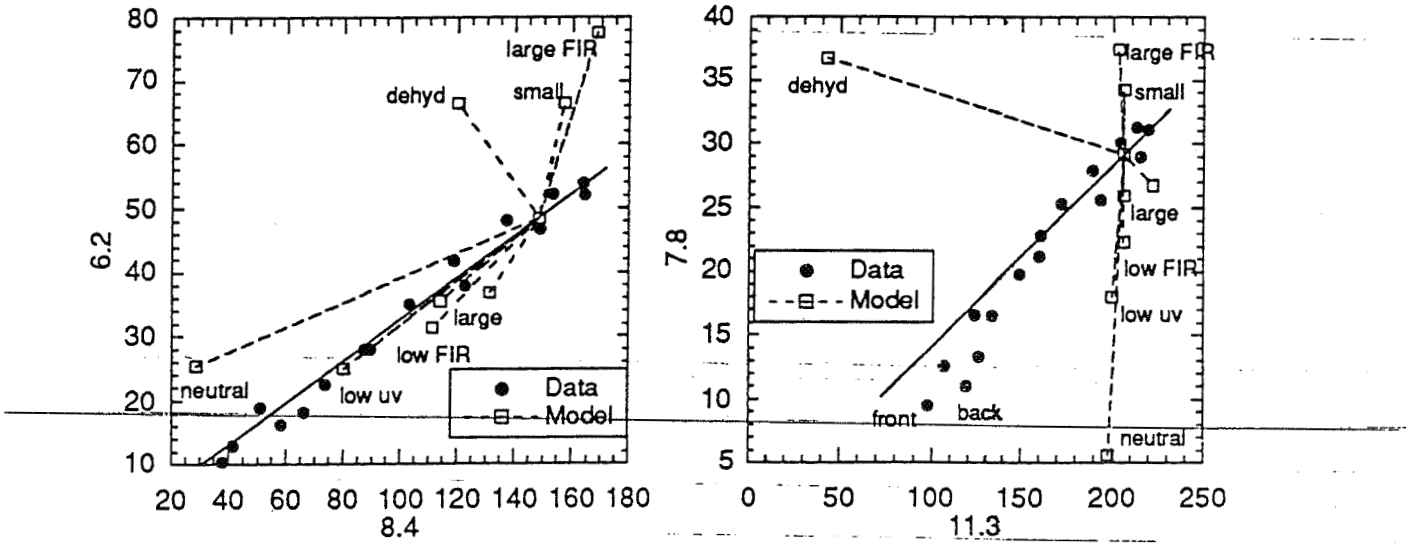

Figure 1c (left) shows the excellent correlation between the C-C mode band intensities as measured at 6.2 and 8.4 μm. Figure 2 (right) shows the correlation between the band intensities of the C-C mode measured at 7.8 μm and the 11.3 μm C-H mode.

consistent with emission expected from lower UV flux regions. The model predicts similar behavior for the 7.8 vs. 8.4 μm data even though the data appear to sample the same emission band. Fig. 1b shows that the 7.8 vs. 8.4 μm data follows the model predictions. The 6.2 and 8.4 μm data (Fig. 1c) are highly correlated, showing almost no deviation from the 1:1 trend line. The model variables which might have accounted for the previous plots (low UV and larger PAHs) move the data points nearly parallel to the 1:1 trend line and thus have little effect in this plot. We thus conclude that the distribution of emission from the C-C mode in PAHs is well represented by the 8.4 μm image. These correlations are also strong support for the identification of PAHs as the source of the emission bands.

C-H Modes

The C-C vs C-H mode plots are good tests of dehydrogenation of the molecules. It is possible that the UV field in some objects is intense enough that the some of the hydrogen atoms will be removed from the PAH molecules. Figure 2 shows the comparison of the 7.8 μm C-C mode with the 11.3 μm C-H mode. The data deviates from the 1:1 trend line, but not in the direction expected if dehydrogenation is significant. The data are instead consistent with the previous plots, where molecule size variations or attenuation of the UV field are adequate to explain the results.

CONCLUSIONS

1. The 6.2 and 8.4 μm data correlate extremely well, in good agreement with predictions of the PAH fluorescence model of Schutte et al. (1993).
2. The other data are consistent with our previous findings (Bregman et al. 1994) that there are variations in the PAH size distribution within the Bar and that the the front of the Bar has a larger size distribution while the back of the Bar shows the effects of a lower UV intensity.
3. As in our previous results, there is no evidence for dehydrogenation of the PAH molecules.

REFERENCES

Bregman, J.D., Larson, K., Rank, D., and Temi, P. 1994, Ap. J., 423, 326.
Schutte, W.A., Tielens, A.G.G.M., and Allamandola, L.J. 1993, Ap. J., 415, 397.

Administrative Display

Functions:

Record 1 of 6
FIRST PREVIOUS NEXT LAST

D017C: No Copyright
D035Z: 96N13684
D039B: 20080427
D039H: 19950830
D039I: Metadata modified
D039J: STI
D041A: English
D072A: 93
D072B: SPACE RADIATION
D090A: 19960003674
D090F: 1996103674
D090H: 350003674
D245A: **Observations of localized** NiII emission in M82: Evidence for supernovae activity in the molecular cloud east of the nucleus
D260C: 19950101
D260D: JAN 1, 1995
D260G: 1995
D260Z: United States
D300A: 4
D355A: Unclassified
D359A: Publicly available
D359C: Unlimited
D359X: Yes
D359X_NOTE: Public dissemination by NTIS confirmed
D359X_DATE: 20080512
D509A: Conference Paper
D520B: Narrow band images of M82 at wavelengths of 6.63 microns (NiII) and 6.8 microns (continuum) are discussed in terms of new evidence for supernova activity in the nuclear region of the M82 starburst galaxy. Data were recorded using a 128x128 Si:Ga array in an infrared camera on the KAO Southern Expedition in April '94.
D520Q: English
D520Z: Author
D541O: Hardcopy
D590A: In Astronomical Society of the Pacific, Airborne Astronomy Symposium on the Galactic Ecosystem: From Gas to Stars to Dust, Volume 73 p 437-440 (SEE N96-

13618 02-88)

D592A: Distributed to NTIS

D650A: EMISSION SPECTRA; GALACTIC NUCLEI; INFRARED ASTRONOMY; INFRARED SPECTRA; LINE SPECTRA; MOLECULAR CLOUDS; STARBURST GALAXIES; SUPERNOVAE

D659A: KUIPER AIRBORNE OBSERVATORY; LUMINOSITY; NICKEL; RATES (PER TIME)

D700A: Rank, David M.; Temi, Pasquale; Bregman, Jesse D.; Dunham, Edward W.; Harker, David

D700E: FROM; FROM; FROM; FROM; FROM

D710A_AA: California Univ.; California Univ.; NASA Ames Research Center; NASA Ames Research Center; NASA Ames Research Center

D710G_AA: United States; United States; United States; United States; United States

D710U_AA: Santa Cruz, CA., United States; Santa Cruz, CA., United States; Moffett Field, CA, United States; Moffett Field, CA, United States; Moffett Field, CA, United States

D710A_FS: NASA

D710G_FS: United States

D710J_FS: NASA

D710U_FS: United States

D710A_OS: NASA Ames Research Center

D710B_OS: FROM

D710G_OS: United States

D710U_OS: Moffett Field, CA, United States

D7106_OS: NC473657

D773P: p 437-440

D773T: Astronomical Society of the Pacific, Airborne Astronomy Symposium on the Galactic Ecosystem: From Gas to Stars to Dust, Volume 73

D773W: N96-13618 02-88

D787F: 0

D787G: Analytic Subsidiary

D937A: CASI

D937B: Hardcopy

D937D: A01

PLD: Jan 12, 1996

BLD: Jun 04, 2003

BMD: 20080512

Record 1 of 6

FIRST PREVIOUS NEXT LAST

Airborne Astronomy Symposium on the Galactic Ecosystem
ASP Conference Series, Vol. 73, 1995
M.R. Haas, J.A. Davidson, and E.F. Erickson (eds.)

Observations of Localized Ni II Emission in M 82: Evidence for Supernovae Activity in the Molecular Cloud East of the Nucleus

D. Rank and P. Temi

Astronomy Department, University of California, Santa Cruz, CA 95064

J. Bregman, E. Dunham, and D. Harker

NASA - Ames Research Center, Moffett Field, CA 94035

Abstract. Narrow band images of M82 at wavelength of 6.63 μm (NiII) and 6.8 μm (continuum) will be discussed in terms of new evidence for supernova activity in the nuclear region of the M82 starburst galaxy. Data were recorded using a 128x128 Si:Ga array in an infrared camera on the KAO Southern Expedition in April '94.

1. Introduction

Supernovae play a key role in the dynamics, structure, and chemical evolution of galaxies. The massive stars that end their lives as supernovae live for short enough times that many are still associated with dusty star formation regions when they explode, making them difficult to observe at visible wavelengths. In active star forming regions (galactic nuclei and starburst regions), dust extinction is especially severe. Thus, determining the supernova rate in active star forming regions of galaxies, where the supernova rate is expected to be one or two orders of magnitude higher than the average, has proven to be difficult. For normal galaxies, the supernova rate varies with type, but is in the range of 1-4 SNU where a SNU is the number of supernovae per 100 years per 10^{10} $L_{\odot}$ in blue luminosity. From observations of SN1987A we know that the [NiII] 6.63 μm emission line was the strongest line in the infrared spectrum for a period of a year and a half after the explosion. Since dust extinction is much less at 6.63 μm than at visible wavelengths ($A_{6.63}/A_V = 0.025$), the NiII line can be used as a sensitive probe for the detection of recent supernovae.

2. Observations

We present new multispectral images of M82 which were taken on the KAO using our 128x128 Si:Ga infrared camera. We used narrow band filters centered at the 6.63 μm NiII line and at 6.8 μm continuum wavelength. The reduction of the data includes all our images of M82 from the April 94 flight. The pointing of the telescope was independently derived by digitizing the KAO guider TV images. The average centroid position of the offset guide star was then used

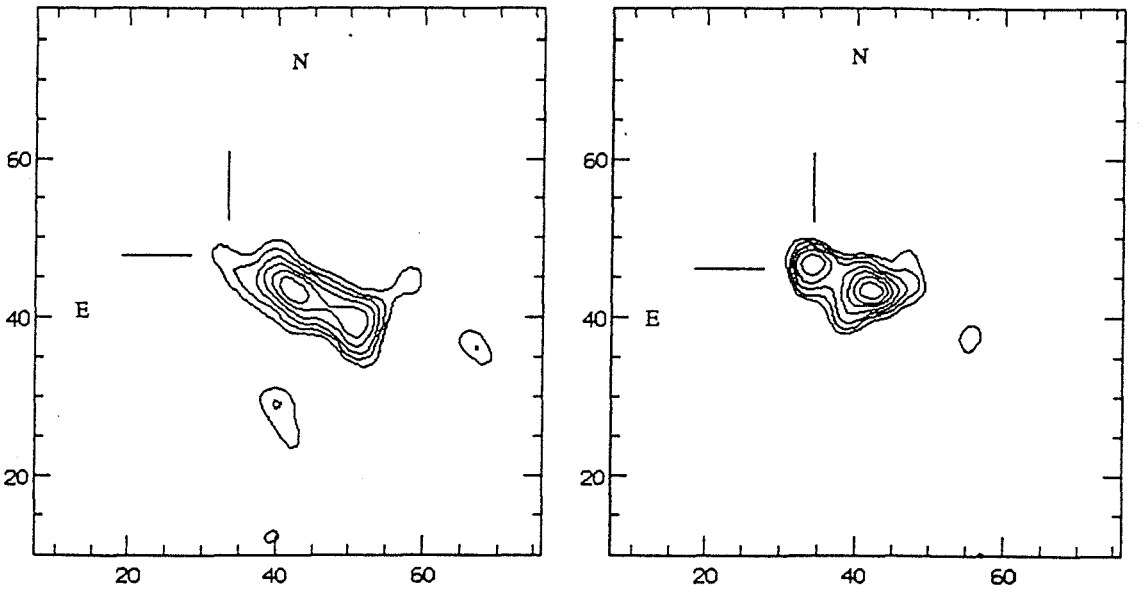

Figure 1. 6.8 μm (left) and 6.63 μm (right) images of M82. The eastern NiII source is indicated by the tick marks. Approximately 20 individual frames have been coadded with a 2.5 pixel (5 arcseconds) smoothing. Absolute positioning on the sky is within 2-3 pixels. $\delta\lambda/\lambda$ = 2.3%

to superimpose each LOS freeze frame image at a fixed rotation angle. From an analysis of the guide star errors and the IR images we have determined that the error in this procedure is about 2-3 pixels in the IR image. The images in Figures 1 and 2 are presented in a common reference frame as referred to the IR pixels on the chip.

Our new observations show clear evidence for NiII emission from the eastern side of the molecular cloud which surrounds the star burst region of the galactic core in M82 (see Figures 1 and 2). The 6.63 μm image shows an unresolved source, in the plane of the galaxy, 15-20 arcseconds to the east of the nucleus at the position of a dark dust lane in optical images. The NiII source shows up as an extension of the core emission in the images taken at the other wavelengths.

3. Discussion

Our observations would imply a large NiII line luminosity for the eastern source which is several million times the luminosity of the sun. Follow-up spectra of the eastern source taken a few weeks later with the KAO confirm our observations of NiII emission (Witteborn 1994). Thus we may have detected the infrared signature of a recent bright supernova in M82. If the observed source is a supernova, it is 100 times brighter than SN1987a in the NiII line, quite a surprise but not impossible. A second perhaps more common but also unexpected explanation for this observation is that the NiII emission arises in gas heated by supernova driven shocks or photo-dissociation regions which are concentrated near the center of the galaxy. These sources would likely be associated with the star burst activity of the nucleus.

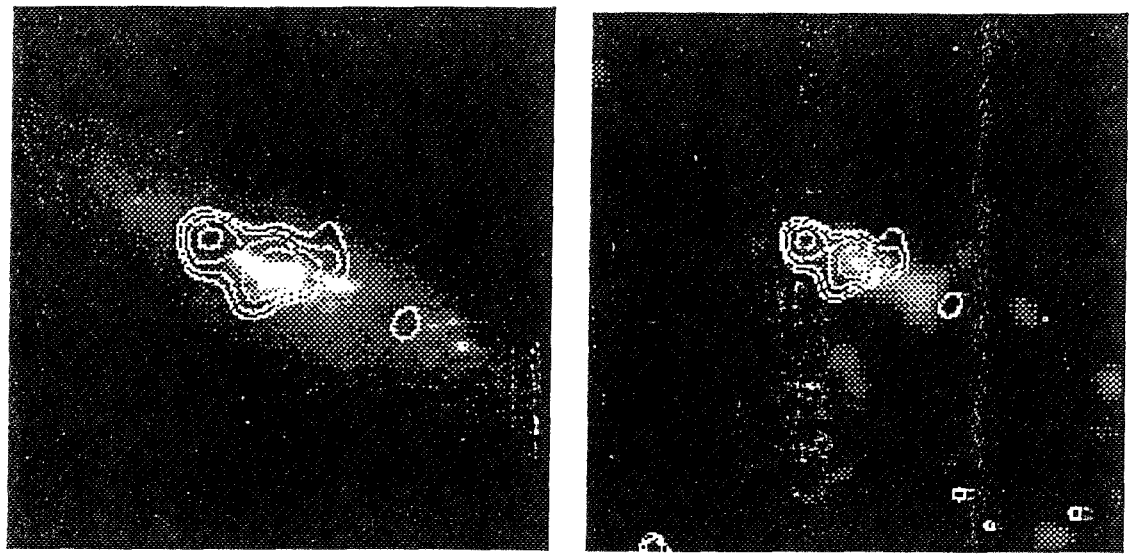

Figure 2. (left) 6.63 μm NiII image of M82 (contour) superimposed on a 1.6 μm FeII narrow band ground based image. It can be seen that the eastern NiII source coincides with a dark lane associated with a molecular cloud just outside the nuclear region of the galaxy. (right) 6.63 μm image superimposed on the 6.8 μm continuum image of Figure 1 showing the absolute registration of the galactic core.

If the NiII emission which we see in the eastern source of M82 is due to a supernova then a NiII/ArII line ratio of 1 or larger should be observed, based on our interpretation of previous IR spectroscopic data; Witteborn (1993) measured roughly equal line strengths for NiII and ArII in the ejecta of SN1987a. Such a large NiII/ArII line ratio is not observed in galactic HII regions where the Ni is depleted by the formation of solid dust grains. Lester et al. (1990), have observed strong FeII emission at 1.6 μm which is fairly uniformly distributed across the core of M82. The ratio of FeII/H lines is 100 times that seen in typical HII regions. These authors conclude that the FeII emission arises in gas heated by supernova driven shocks rather than in photo- dissociation regions which are concentrated at the center of the galaxy. Thus the FeII seen in their spectra is thought to be the result of sputtering of dust grains in the shocked gas. An integrated FeII luminosity of $5\text{x}10^5$ $L_\odot$ for M82 is derived from their data. Our observations would imply an even larger NiII luminosity of $5\text{x}10^6$ $L_\odot$ for the eastern source in M82. We see a marked difference between the eastern and western sources in the 6.6 μm NiII line luminosity. The two sources have nearly equal FeII luminosities in Lester's 1.6 μm data. Thus the eastern source may be intrinsically much brighter than the western source in these two metalic lines, but extinction surrounding M82's core substantially diminishes the flux at 1.6 μm.

References

D.F. Lester, J.S. Carr, M. Joy, and N. Gaffney, 1990, ApJ, 352,544

F. Witteborn, 1993, 1994 private communication

Brief Display

Functions:

Record 1 of 1
FIRST PREVIOUS NEXT LAST

Mid-infrared array camera on the KAO

Document Type: Conference Paper

Author Information: Bregman, Jesse D.; Harker, David; Rank, David M.; Temi, Pasquale

Abstract: The University of California at Santa Cruz and the NASA Ames Research Center have developed a mid-infrared Si:Ga 128 x 128 array camera. The camera has been used on several flights on the KAO to obtain data in the mid-infrared wavelength (4-8 micron) range. At the f/17 bent Cassegrain focus, the pixel spacing is 1.6 arcsec, resulting in a FOV of 3.4 arcmin. The bandpass of the camera is determined by a set of 4 fixed filters and a 4-8 micron CVF. Camera performance of 92mJy/square arcsec/minute has been achieved, but is far from optimal. Realistic improvements to the camera and pointing stability on the KAO in the near future should increase the camera's sensitivity on future flights by 5-10x.

Publication Date: JAN 1, 1995

Document ID (CASI): 19960003701

Accession Number: 96N13711

Security Classif.: Unclassified

Restriction on Access: Unlimited

Authorized Users: Publicly available

Copyright Indicator: No Copyright

Description: 4p

Source Publication: Astronomical Society of the Pacific, Airborne Astronomy Symposium on the Galactic Ecosystem: From Gas to Stars to Dust, Volume 73/ p 583-586/ (SEE N96-13618 02-88)

Imprint and Other Notes: In Astronomical Society of the Pacific, Airborne Astronomy Symposium on the Galactic Ecosystem: From Gas to Stars to Dust, Volume 73 p 583-586 (SEE N96-13618 02-88),Distributed to NTIS

Available From: CASI

Format and Price Code: Hardcopy - Price Code: A01

Record 1 of 1
FIRST PREVIOUS NEXT LAST

Airborne Astronomy Symposium on the Galactic Ecosystem
ASP Conference Series, Vol. 73, 1995
M.R. Haas, J.A. Davidson, and E.F. Erickson (eds.)

MID-INFRARED ARRAY CAMERA ON THE KAO

Jesse Bregman and David Harker

NASA - Ames Research Center, Moffett Field, CA 94035

D. Rank and P. Temi

Astronomy Department, University of California, Santa Cruz, CA 95064

Abstract. The University of California at Santa Cruz and the NASA Ames Research Center have developed a mid-infrared Si:Ga 128x128 array camera. The camera has been used on several flights on the KAO to obtain data in the mid-infrared wavelength (4-8μm) range. At the f/17 bent Cassegrain focus, the pixel spacing is 1.6 arcsec, resulting in a FOV of 3.4 arcmin. The bandpass of the camera is determined by a set of 4 fixed filters and a 4-8μm CVF. Camera performance of 92mJy/square arcsec/minute has been achieved, but is far from optimal. Realistic improvements to the camera and pointing stability on the KAO in the near future should increase the camera's sensitivity on future flights by 5-10x.

1. Instrument Description

The introduction of large scale two dimensional infrared arrays is in the process of revolutionizing observational astronomy. We have extended this technology to mid-infrared wavelengths for spectroscopic imaging with the KAO. An Amber Engineering Inc. 128x128 Si:Ga detector is currently in operation in our mid-infrared camera. The camera is designed around a LHe dewar with an optical design shown in Figure 1. Anti-reflection coated lens, filter, and window assemblies, which are optimized for the bandpasses used, are modular in construction, allowing a change of array and optics in a few hours. The camera has a filter wheel with four fixed filters and a 2% CVF (4-8μm), a 38mm f/1.5 ZnSe reimaging lens operating at a focal reduction of 2, and Lyot stop baffles.

On the KAO, the camera is mounted at the bent Cassegrain focus (f/17), providing a pixel spacing of 1.6 arcsec and a FOV of 3.4 arcmin. This large FOV allows for chopping between two areas on the array when the sources are less extended than about an arcmin. The light path between the instrument and the air bearing is enclosed in a pipe which allows cold air to be drawn from the telescope cavity, past the beamsplitter, and vented overboard. This arrangement reduces the effective temperature gradient between telescope and camera, thereby improving the image quality and reducing the background as seen by the detector.

The array can be read in the stare and integrate mode or in phase with the chopper. The chopped data are coadded in two separate frame buffers. DC sky

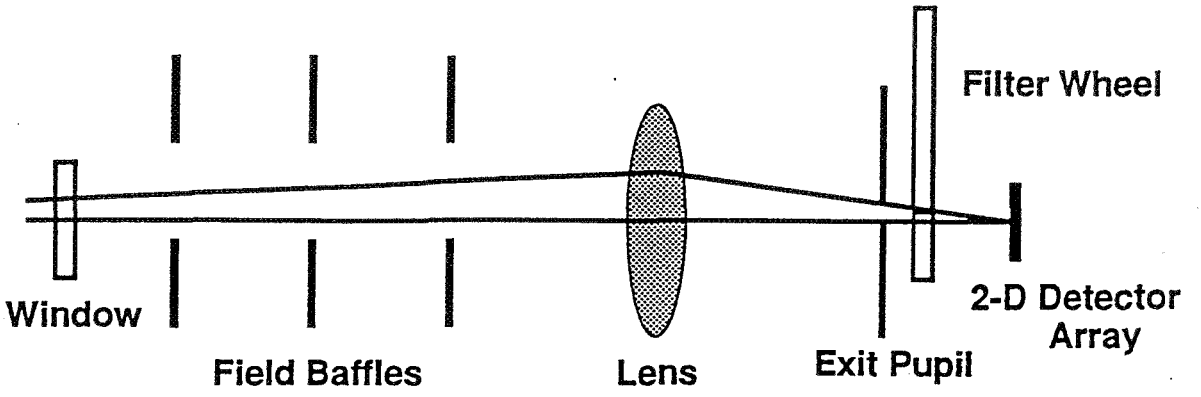

Figure 1. Optical layout of the spectrographics camera. The system is well baffled to assure low background and the exit pupil stop has a central blocking spot ($\approx$ 10% in area) which is matched to the telescope's central obscuration, thus eliminating direct thermal radiation from high emissivity surfaces.

and "flat" frames, which are used to calibrate the array, are stored separately at the beginning of data taking. We record the frame buffer data at intervals of 10 to 60 seconds as part of the data acquisition sequence, much as we do for our ground based observations. For on chip chopping, subtraction of the buffers produces a double image of the source minus the sky. This technique has the advantage of continuous measurement of the sky background and nearly 100% duty cycle for the focal plane light.

A block diagram of our portable data system is shown in Figure 2. Instrument control, data acquisition, and on-the-spot reduction are performed by a Macintosh IIx computer. A National Instruments I/O board provides the master clock timing signals to the array controller and computer interface electronics. Parallel 12 bit focal plane array data from the controller is captured by a second National Instruments digital I/O board and placed directly into memory for access by the Macintosh using both custom software and several commercial software packages. We also use an ethernet link to secondary computers so that IRAF can be used to process the data in near real time. The ethernet link is used with the Sun computers on the KAO for data reduction and backup storage.

To account for the rotation of the images, data are collected in the KAO's "freeze mode" in which many frames can be taken at one angle of rotation. The data are then later derotated in the reduction process. An example of the KAO stellar profile from the data at 6.2μm obtained on our April 1, 1994 flight is shown in Figure 3. The greyscale picture is of our standard, Alpha Ori, and the graph is a radial profile of the star.

2. Instrument Performance

Performance measurements were made of the Si:Ga camera at 6.6μm on the KAO during flights in March and April 1994. We have achieved a 50 pixel (12.8″ circle at 1.6″/pixel) sensitivity of $\approx 5 \times 10^{-19}$ W/cm^2 = 1 sigma rms in 330 sec or 92mJy/sq arcsec/min ($\Delta\lambda/\lambda = 40$).

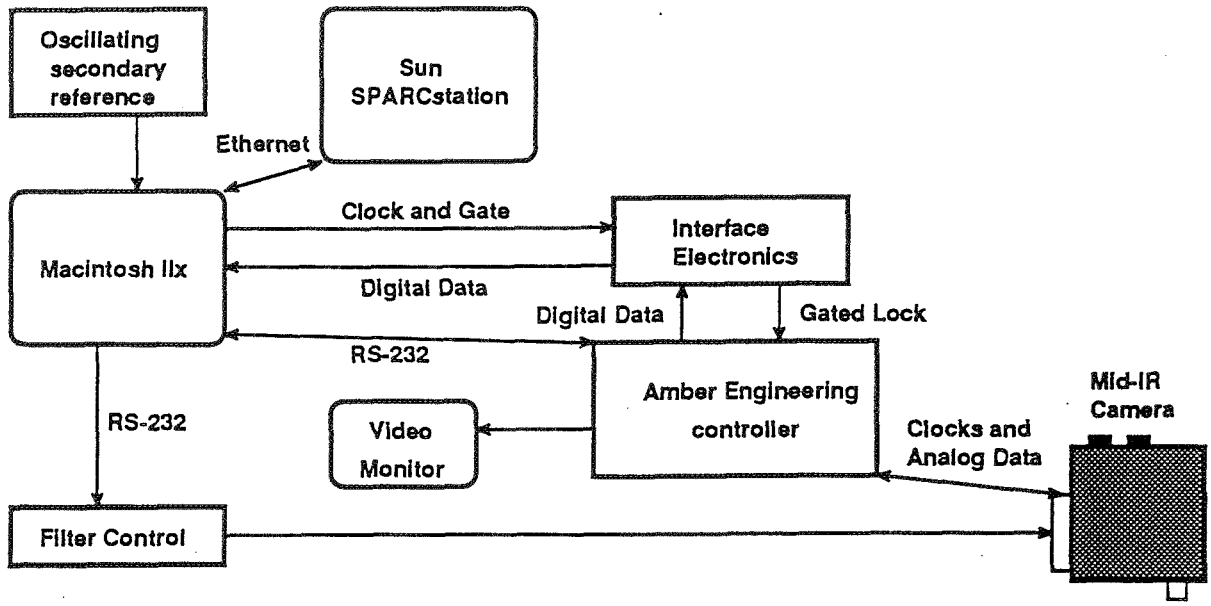

Figure 2. Block diagram of the present data taking system as it is installed on the KAO

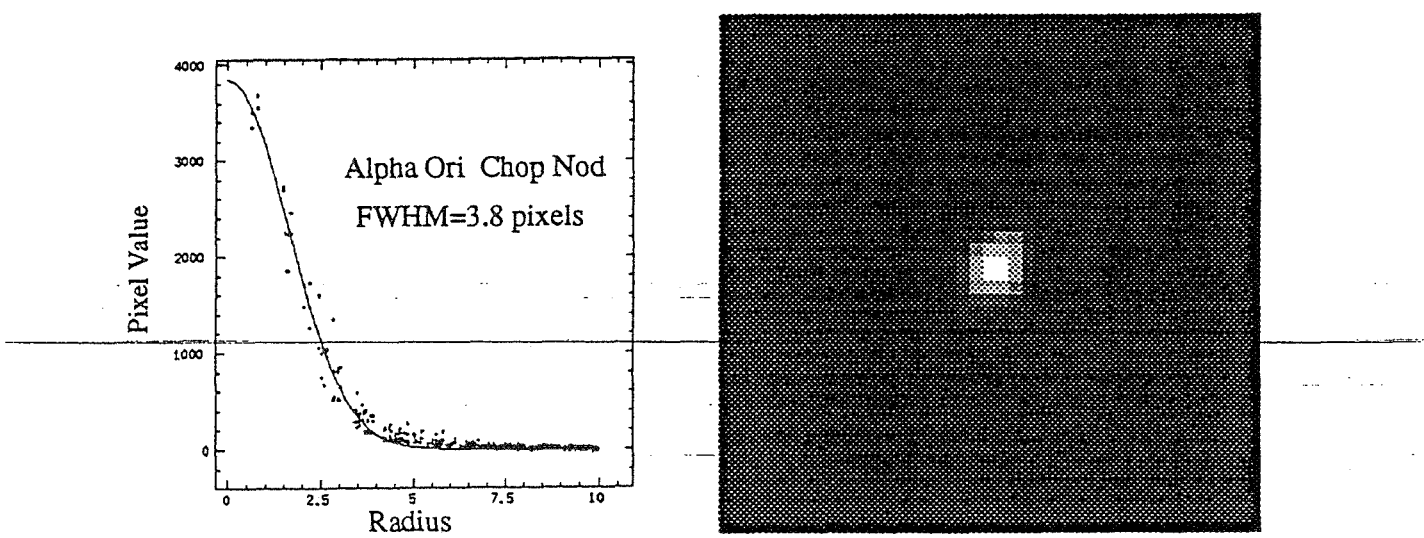

Figure 3. KAO stellar profiles of Alpha Ori. On the left is a profile taken on 4/1/94 at 6.2μm in a chop and nod sequence of four integrations, $+--+$ with the camera. On the right is a 64x64 section of the chip from which the profile is taken. The 6.2μm profile has a FWHM of 6.1 arcsec. This image size is mostly a measure of the tracker chop-nod stability of our flight.

This performance is more than an order of magnitude worse than for an optimized system (*i.e.* BLIP).We have identified two problems which degraded the camera sensitivity. First, the background power we measured was 14 times higher than for a 240K telescope with an emissivity of 10%. Secondly, the CVF we used had a transmission of only 20%. We can reduce the background substantially by changing the way we mount the camera, and we will improve the filter transmission by using fixed filters with peak transmission of 80%. In addition, the pointing stability of the telescope was poor, resulting in point source images spread over a diameter of 8 pixels (13 arcsec). We know from seeing experiments that the FWHM of a point source should be 3 arcsec. Image motion compensation (work now underway on the KAO) should additionally improve our total point source S/N by about 2x. Thus, we realistically expect a point source sensitivity improvement of 5-10 times that measured on our last flight, or 2×10^{-18} W/cm^2 = 5 sigma in 10 seconds.

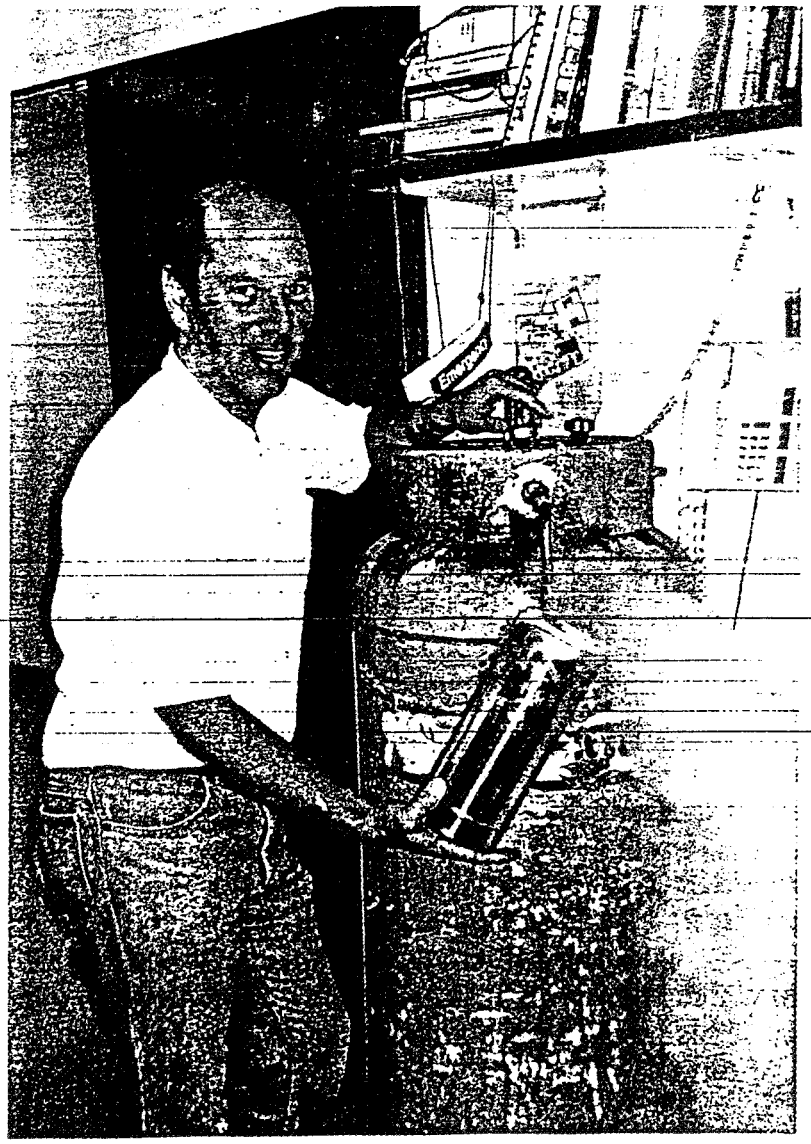

Jesse Bregman

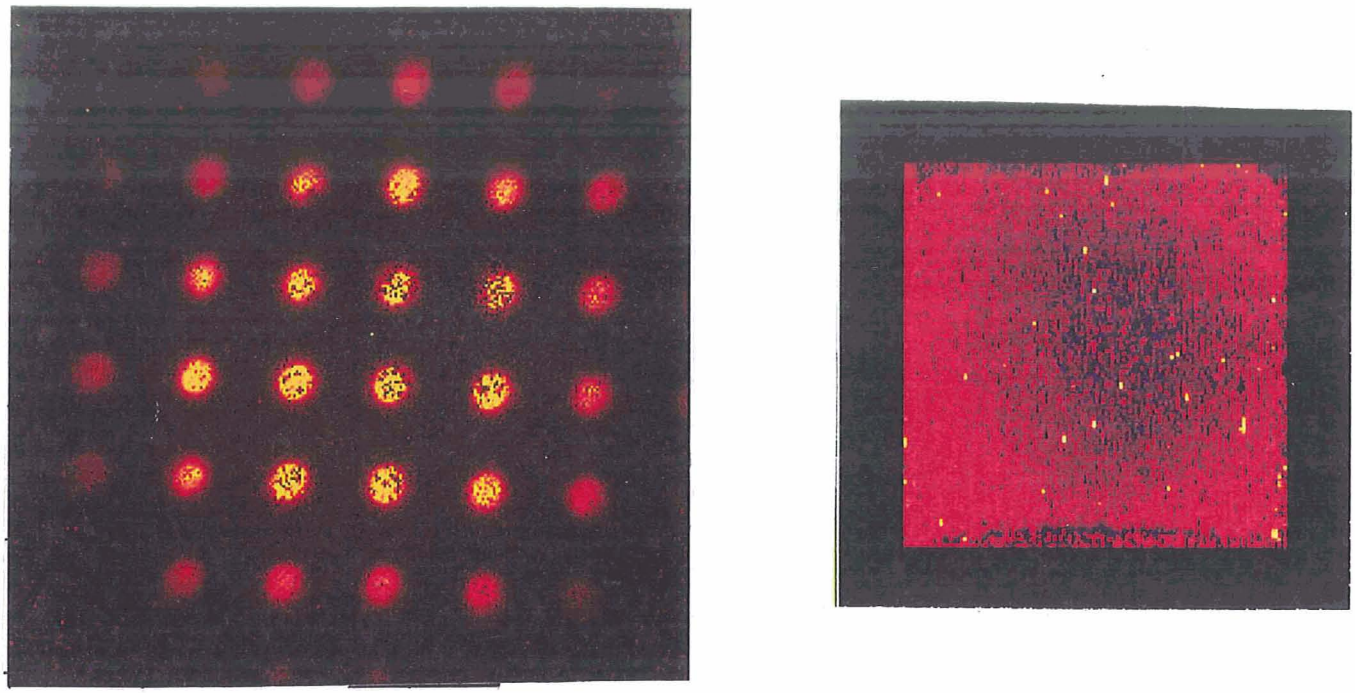

Figure 1. Laboratory images produced by long wavelength HgCdTe infrared detector arrays from Amber Engineering Inc. The image on the left is from a 256x256 array with a 10.5 micron long wavelength cutoff while the one on the right was generated using a 128x128 array with an 11.5 micron cut off wavelength. Dark current at 40K is a strong function of cutoff wavelength ranging from 10^5 e/sec to 10^3 e/sec for 11.5 and 9 micron cutoff wavelengths respectively.